Supporting Information

Wen et al. 10.1073/pnas.1309354110

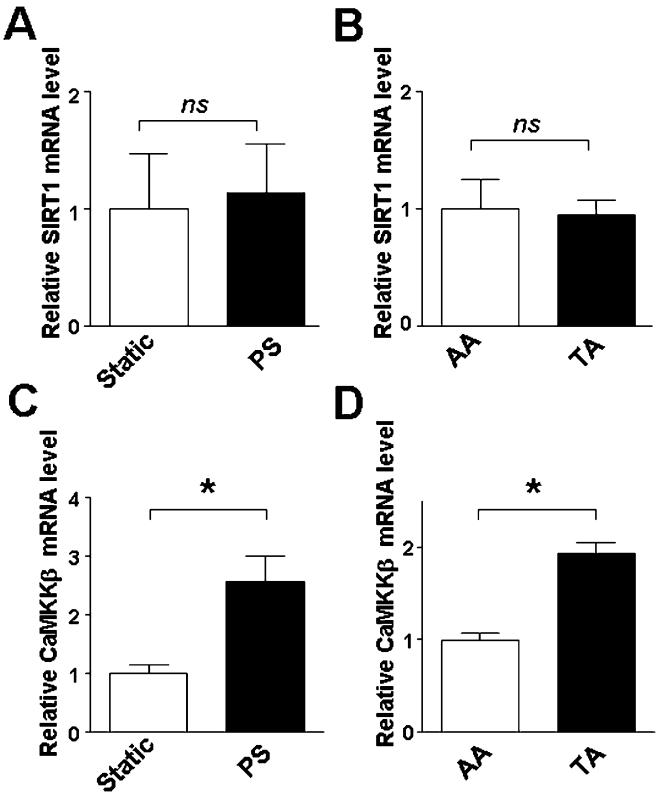

Fig. S1. Pulsatile shear stress (PS) increases Ca^{2+}/calmodulin-dependent protein kinase kinase (CaMKK)β mRNA but has little effect on Sirtuin (SIRT)1 mRNA in vitro and in vivo. The levels of SIRT1 mRNA (*A* and *B*) and CaMKKβ mRNA (*C* and *D*) in the human umbilical vein endothelial cells (HUVECs) exposed to static or PS (*A* and *C*) and in the thoracic aorta (TA) and aortic arch (AA) regions of the wild-type mice (*B* and *D*). The results are the means ± SEM of at least three independent experiments in *A* and seven animals in *B*. *$P < 0.05$; ns, no statistical difference.

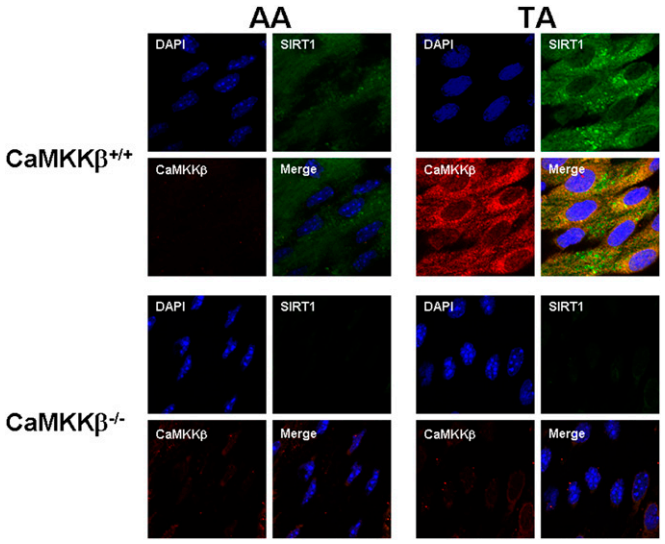

Fig. S2. Topographic expression of SIRT1 in mouse aorta depends on CaMKKβ. AA and TA were isolated form CaMKKβ$^{-/-}$ mice and their CaMKKβ$^{+/+}$ littermates. SIRT1 and CaMKKβ were detected *en face* with the corresponding antibodies followed by Alexa Fluor 488 goat anti-mouse IgG or rhodamine (TRITC)-conjugated goat anti-rabbit IgG. The nuclei were counterstained with DAPI. Images were acquired using an Olympus FV1000 confocal microscope. DAPI, FITC, and TRITC fluorophores were excited at 405, 488, and 559 nm.

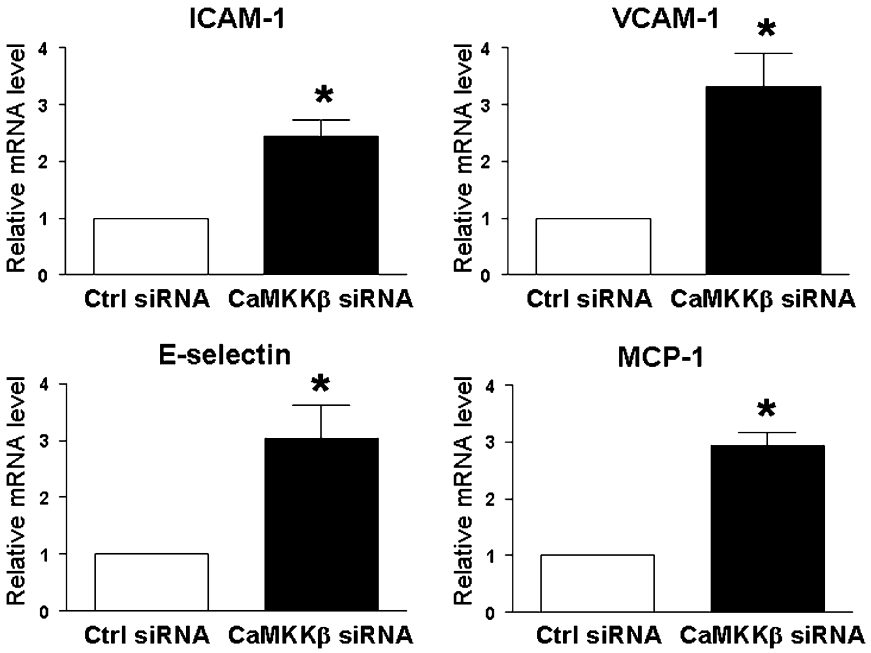

Fig. S3. PS suppression of proinflammatory genes is CaMKKβ-dependent. HUVECs were transfected with control siRNA or CaMKKβ siRNA (10 nM) and then exposed to PS for 8 h. The levels of intercellular adhesion molecule (ICAM)-1, vascular cell adhesion molecule (VCAM)-1, E-selectin, and monocyte chemotactic protein (MCP)-1 mRNA were detected and normalized to that of β-actin. The results are the means ± SEM of at least three independent experiments. *$P < 0.05$.

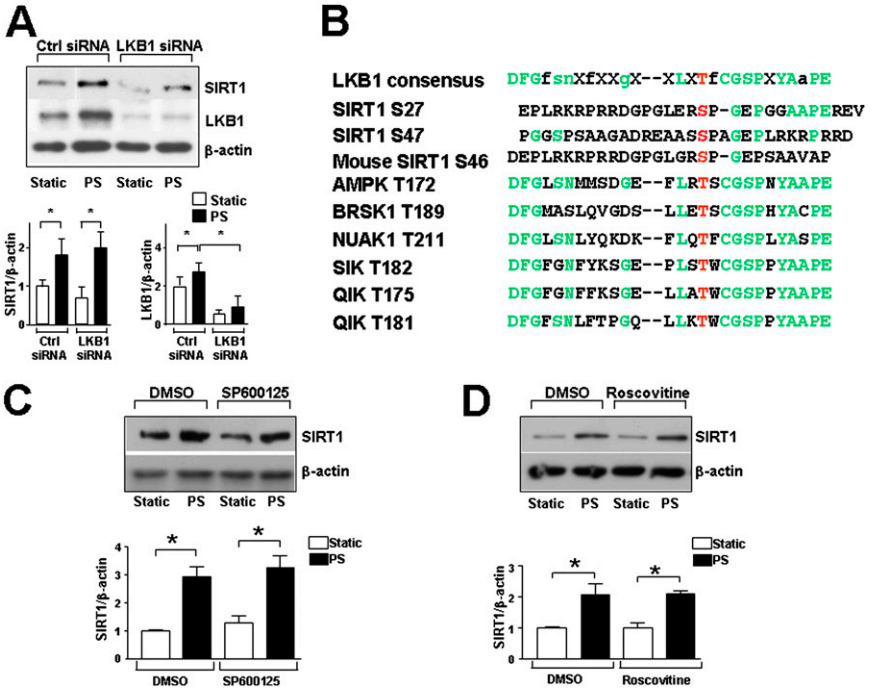

Fig. S4. Liver kinase (LK)B1, JNKs, and cyclin-dependent kinase (CDK)5 are not involved in SIRT1 regulation by PS. (*A*) SIRT1 and LKB1 levels in HUVECs transfected with control siRNA or LKB1 siRNA (10 nM) and then exposed to PS for 8 h or kept under static conditions. Bar graphs to the right summarize the mean ± SEM results of three independent experiments. $*P < 0.05$. (*B*) Alignment of LKB1 substrate consensus sequences with peptide sequences flanking human SIRT1 Ser-27, human SIRT1 Ser-47, mouse SIRT1 Ser-46, AMP-activated protein kinase (AMPK) Thr-172, brain specific serine/threonine kinase (BRSK)1 Thr-189, NUAK1 Thr-211, SIK Thr-182, Qin-induced kinase (QIK) Thr-175, and QIK Thr-181. Capitalization indicates the highly conservative residues. (*C* and *D*) HUVECs were pretreated with 10 μM SP600125 (*C*), 10 μM Roscovitine (*D*), or DMSO for 30 min and then subjected to PS for 8 h. SIRT1 level in HUVECs were determined by immunoblotting. The bar graphs below summarize the means ± SEM from at least three independent experiments.

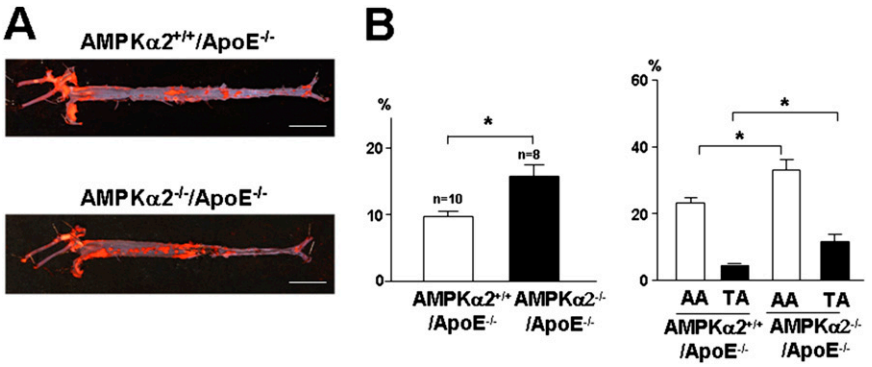

Fig. S5. AMPKα2 ablation increases atherosclerosis in apolipoprotein (Apo)$E^{-/-}$ mice. (*A*) Macrophotographs of oil red O-stained aorta from AMPKα$2^{+/+}$ $ApoE^{-/-}$ and AMPKα$2^{-/-}$$ApoE^{-/-}$ mice fed a Paigen diet for 12 wk. (Scale bar: 0.5 cm.) (*B*) Quantification of the results shown as the mean ± SEM of the aortic specimens with the indicated number of animals. Quantification of percentage of lesion areas in the whole aorta (*Left*) and AA and TA (*Right*). $*P < 0.05$.

Table S1. Values of SIRT1 pSer27 main sequence ions

pSer27 main sequence ions	*m/z*
b ion	
b1	N/A
b2	201.1
b3	272.1
b4	359.2
b5	446.2
b6	543.2
b7	614.3
b8	671.3
b9	800.3
b10	897.4
b11	1,010.5
y ion	
y1	175.1
y2	288.2
y3	385.3
y4	514.3
y5	571.3
y6	642.4
y7	739.4
y8	826.4
y9	913.5
y10	984.5
y11	1,055.5

Low-energy collision-induced dissociation was used for fragmentation to generate b and y ions. *m/z*, mass-to-charge ratio; N/A, not available.

Table S2. Values of SIRT1 pSer47 main sequence ions

pSer27 main sequence ions	*m/z*
b ion	
b1	N/A
b2	185.1
b3	242.1
b4	371.2
b5	468.2
b6	525.2
b7	582.3
b8	653.3
b9	724.3
b10	821.4
b11	950.4
y ion	
y1	175.1
y2	304.2
y3	401.2
y4	472.3
y5	543.3
y6	600.3
y7	657.3
y8	754.4
y9	883.4
y10	940.4
y11	1,037.5

Low-energy collision-induced dissociation was used for fragmentation to generate b and y ions. *m/z*, mass-to-charge ratio; N/A, not available.

Table S3. Serum lipid profile of CaMKKβ$^{-/-}$/ApoE$^{-/-}$ and their CaMKKβ$^{+/+}$/ApoE$^{-/-}$ littermates

Serum lipids	CaMKKβ$^{+/+}$ApoE$^{-/-}$, mg/dL (n = 6)	CaMKKβ$^{-/-}$ApoE$^{-/-}$, mg/dL (n = 6)
TC	2,899 ± 188	2,875 ± 160
TG*	269 ± 73	263 ± 7
LDL-C	1,875 ± 179	1,881 ± 4179
VLDL-C	53 ± 7	53 ± 5
HDL–C†	678 ± 96	624 ± 88

All values are expressed as means ± SEM averaged from six animals in each group. HDL-C, HDL–cholesterol; LDL-C, LDL–cholesterol; TC, total cholesterol; TG, triglyceride; VLDL-C, very-low-density lipoprotein–cholesterol.
*The TG value is divided by 5 to estimate VLDL-C levels.
†The HDL-C value was determined by the following formula: HDL-C = (TC − LDL-C − TG)/5.

Table S4. Serum lipid profile of EC-SIRT1$^{-/-}$/ApoE$^{-/-}$ and their EC-SIRT1$^{+/+}$/ApoE$^{-/-}$ littermates

Serum lipids	SIRT1 EC$^{-/-}$ApoE$^{-/-}$, mg/dL (n = 7)	SIRT1 EC$^{+/+}$ApoE$^{-/-}$, mg/dL (n = 7)
TC	2,466 ± 90	2,366 ± 100
TG*	254 ± 35	247 ± 38
LDL-C	1,826 ± 46	1,916 ± 153
VLDL-C	50 ± 7	49 ± 7
HDL-C†	566 ± 91	556 ± 58

All values are expressed as means ± SEM averaged from number of animals as indicated. EC, endothelial cell.
*The triglyceride value is divided by 5 to estimate VLDL-C levels.
†The HDL-C value was determined by the following formula: HDL-C = (TC − LDL-C − TG)/5.